Crystallographic and magnetic study of metastable nanocrystalline $Sm(Fe,Si)_9$

C. Djéga-Mariadassou, L. Bessais, and A. Nandra
LCMTR, UPR209, CNRS, 2/8 rue Henri Dunant, B.P. 28 F-94320 Thiais, France

E. Burzo
Facultatea de Fizica, Universitatea Babes-Bolyai, 3400 Cluj-Napoca, Romania

(Received 25 November 2002; revised manuscript received 11 February 2003; published 9 July 2003)

We have studied nanocrystalline metastable $P6/mmm$ $Sm(Fe,Si)_9$ by means of x-ray diffraction, Mössbauer spectroscopy coupled with Curie temperature and magnetization measurements. The structural transformation towards equilibrium $R\bar{3}m$ $Sm_2(Fe,Si)_{17}$ is studied by Rietveld analysis. A decreasing unit cell volume for substituting Fe by Si was found. The Curie temperature increases with Si content with a slight improvement of the magnetic moment per iron atom compared to the equilibrium $Sm_2(Fe,Si)_{17}$ alloys. A specific program for the Wigner-Seitz cell calculation of the metastable disordered structure was used. The hyperfine parameter sets were assigned according to the relationship between the Wigner-Seitz cell volume of each iron site and their isomer shift. It results that Si preferentially occupies the $3g$ site with the recurrent sequence $H_{HF}(2e) > H_{HF}(6l) > H_{HF}(3g)$. The mean hyperfine field decreases with silicon content.

DOI: 10.1103/PhysRevB.68.024406 PACS number(s): 75.50.Bb, 75.50.Tt, 76.80.+y

I. INTRODUCTION

A metastable phase is not the most thermodynamically stable phase, but a temporarily stable one under certain conditions. The metastable phase forms under conditions corresponding to a local minimum of the free energy. The metastable phases open a way of searching for novel permanent-magnet materials. One of the motivations of the investigations is the outstanding magnetic properties that are important for practical applications. Furthermore, the study of the formation of metastable phases and their transformation into the various equilibrium phases is most important to reach a better understanding of the relation between crystal structure and intermetallic thermodynamic stability.

A new generation of permanent magnets came into view when an interstitial atom was introduced in some *R*-Fe lattice. Among the most interesting compounds, the Sm_2Fe_{17} rhombohedral alloy of the Th_2Zn_{17} structure type with an interstitial modified structure has generated much enthusiasm after the first discovery of $Sm_2Fe_{17}N_3$. The major drawback to its utilization is its poor thermal stability, as it decomposes into the equilibrium phases SmN and α – Fe above 873 K (Ref. 1). Therefore, worldwide investigations have been made and are still in progress in a quest for Fe substitution or interstitial modifications sufficient to obtain further improvements.

It has been shown most particularly that Al, Ga, and Si improve the thermostability of the Th_2Zn_{17}-type interstitial structure, Si and Ga having the strongest influence.[2] Moreover, high performance magnets result from the coupling of outstanding intrinsic magnetic properties with a convenient microstructure, strongly dependent on the processing method used to prepare the materials. In this context, the road leading to promising candidates includes techniques favoring directly the nanocrystalline state via out-of-equilibrium phases stable up to high temperature. In the case of the Fe-rich Sm alloys, much confusion still remains about the exact nature of the phase mainly responsible for the interesting properties, when sputtering or energetic milling is implemented. For certain preparation temperature conditions, the $P6/mmm$ hexagonal phase derived from $CaCu_5$ and known as $TbCu_7$ is observed. This hexagonal structure sub-cell of Th_2Zn_{17} was found to be more efficient than the materials with the $R\bar{3}m$ super-lattice of Th_2Zn_{17}-type when interstitially N or C filled.[3] For other authors, the optimum magnetic properties are considered as related to the Th_2Zn_{17}-type compounds.[4]

The usual denomination as a $TbCu_7$ structure or a $SmFe_7$ phase[5,6] remains ambiguous as it implies a composition of 2/14 for this precursor, Sm enriched with respect to its derivative structure 2/17. The $TbCu_7$ structure has been considered as a transition-metal-deficient 2/17 structure in which the long-range order of transition metal pairs, known as dumbbells, is absent. Direct results on Sm alloys are not reported owing to the compositional inaccuracy of the samarium samples[7] but, from high-electron-energy diffraction and high-resolution-electron microscopy on Y_2Fe_{17} carbides obtained by arc-melting, it was reported that the disordering of the $TbCu_7$ structure is due to a random stacking of homogeneous iron or yttrium sheets which retain the 2/17 stoichiometry. The x-ray diagrams of the melt spinning and annealing of Sm-Fe based alloys have been indexed on the basis of the Th_2Zn_{17} $R\bar{3}m$ structure, even when the superstructure lines are extremely weak or absent.[8] In contrast, it must be emphasized that several works related to alloys obtained with high energy ball milling and sputtering techniques have shown the existence of $SmFe_9$ phase with the hexagonal $P6/mmm$ structure, precursor of the Th_2Zn_{17} ordered $R\bar{3}m$ phase.[9–11] Teresiak *et al.*[10] proposed a modified $R\bar{3}m$ Th_2Zn_{17} structure to explain the progressive emergence of the superstructure lines, linked to the transition from the subcell hexagonal $CaCu_5$ derived phase $SmFe_9$ to the multiple cell Th_2Zn_{17}.[11] However until this present work, to our knowledge, no one has invoked a possible stoichiometry evolution of the $SmFe_9$ phase towards the 2/17 composition. We shall discuss and comment on this evolution upon Si

effect and in terms of gradual Sm enrichment with annealing temperature.

It appears that the understanding of the structure transformation from the nanocrystalline precursor to the Th_2Zn_{17} structure is still open to discussion. Moreover, the understanding of the host lattice configuration prior to carbonation remains of outmost interest since the high performance magnetic properties of the carbides will be tightly correlated to intrinsic structural characteristics combined with an adequate microstructure of the materials.

In the present work we have prepared the $Sm(Fe,Si)_9$ out-of-equilibrium alloys using a high energy milling technique, which is a cost effective alternative to rapid quenching and allows the production of large batches of homogeneous materials. We shall study the influence of Si content at a given annealing temperature on unit cell parameters, and explain the effect of temperature for a given Si content. The crystallographic information will provide the necessary explanation for the study of intrinsic magnetic properties developed afterwards, i.e., Curie temperature, magnetic moment, and hyperfine parameters. A approach to explain the Mössbauer spectra of such metastable system has been achieved to assign the hyperfine parameters according to a correlation with Wigner-Seitz volumes derived from a new specific algorithm.

II. EXPERIMENT

The samples $Sm_2Fe_{17-x}Si_x$($x=0.5$, 1, 1.5, 2, and 3), with samarium excess, were prepared by the technique of high-energy ball milling and subsequent annealing from 650 °C to 1150 °C during 30 min as described previously.[12]

X-ray diffraction with Cu radiation has been carried out on a Brucker diffractometer with an internal Si standard to insure a unit cell parameter accuracy of $\pm 1\times 10^{-3}$. The intensities were measured from $2\theta=20°$ to $2\theta=110°$ with a step size of 0.04° and counting time of 22 s per scanning step. The structure refinement was performed by the Rietveld technique supported, in the assumption of Thompson-Cox-Hastings line profile, by the FULLPROF computer code. The detailed information was given in Refs. 13–18.

The magnetic ordering temperatures T_C were obtained on a differential sample magnetometer MANICS in a field of 1000 Oe on powder in an evacuated sealed silica tube. Magnetization was measured at 4 K with a VSM magnetometer and an applied field up to 9 T. The Mössbauer spectra with absorbers containing 12 mg/cm^2 of natural iron, were collected at 295 K on a constant-acceleration spectrometer with a rhodium-matrix cobalt-57 source. The spectrometer calibration gives a line-width of 0.25 mm/s for natural iron. The spectra were fitted according to the procedure discussed below with estimated errors of ± 0.1 T for hyperfine fields H_{HF} and ± 0.005 mm/s for isomer shifts δ and quadrupole shifts 2ε.

III. RESULTS AND DISCUSSION

A. Crystallographic studies

According to the annealing temperature, the spectra can be classified into three main families, whose limits vary with Si content. Series (A) annealed at temperature ranging from 650 °C up to around 850 °C for $x=0.5$ and 875 °C for higher Si content, is representative of the hexagonal sub-cell $P6/mmm$ derived from $CaCu_5$. Family (B), annealed at a higher temperature above 900 °C is characterized by the full transformation of the alloys into the Th_2Zn_{17} structure type with the expected intensities of the superstructure extra lines typical of the $R\bar{3}m$ space group (104), (211), (112), (024).[12] The (C) family annealed at temperature between 875 and 900 °C shows the gradual emergence of the superstructure extra lines. Figures 1(a) and 1(b) report such evolution for $x=0.5$ and 2.

The observed unit cell parameter evolution of the hexagonal phase upon Si substitution is correlated to the atom distribution. In order to understand the effect of Si, it is useful first to revisit the model invoked to explain the stoichiometry evolution of the binary RM_5 phase.

1. Route from RM_5 to $R_{1-s}M_{5+2s}$

The stoichiometry variation from RM_5 of $CaCu_5$ type to M enriched phase $R_{1-s}M_{5+2s}$ results from the substitution of s rare earth atoms by s dumbbells $M-M$ according to Givord *et al*'s model[19] for small s values ($s\simeq 0.03$–0.04) (Table I). Nevertheless for higher s, authors generally refer to the $TbCu_7$ structure as given by Pearson[20] which *stricto sensu* matches the composition 1/7. The description given by Pearson, with the atom distribution as given in Table I, is difficult to imagine because it does not take into account the perturbation brought about by the R substitution by the M pair and preserves the special $2c$ Wyckoff positions $(\frac{1}{3},\frac{2}{3},0)$ like for the stoichiometric RM_5 structure. The temptation is to extend Givord's model[19] to the $TbCu_7$ structure ($s=0.22$) with the coexistence of the $2c$ and $6l$ families with correlatively shifted positions $(x,2x,0)$ $x\simeq 1/3$. However, in the Sm-Fe system it has been shown by Rietveld analysis[10,11] that the s value 0.22 which corresponds to the 1/7 ratio is not in agreement with the x-ray intensity data, s was found to be equal to 0.36–0.38, representative of the stoichiometry 1/9. For $s=0.33$, one R atom out of 3 is substituted for by one dumbbell pair; the stoichiometry is equal to 2/17. If the dumbbell pairs $2e$ are randomly distributed, the structure remains hexagonal $P6/mmm$ and the description given even by the extension of the Givord *et al*'s model[19] leads to the vanishing of the $2c$ family, implying the occupation of one third of the $6l$ site, i.e., two atoms per unit cell.[11] However, the ordered substitution of the R atoms by the dumbbell pairs leads to the rhombohedral Th_2Zn_{17} type $R\bar{3}m$ structure. The concentration dependence of the cell parameter for Co super-stoichiometric $SmCo_5$, $Sm_{1-s}Co_{5+2s}$, for small s values, was proposed by Buschow and Van der Goot.[21] It was observed that c increases due to the replacement of the Sm atom by a more voluminous pair Co-Co along the c axis (see Table II). It results in a contraction of the a parameter which brings the Co atoms initially in the $(\frac{1}{3},\frac{2}{3},0)$ position to $(x,2x,0)x<0.33$ towards the empty Sm position. If one makes a comparison between the unit cell parameters of the $SmFe_9$ phase, $y=0$, ($a=4.925$ Å $c=4.160$ Å) and those of

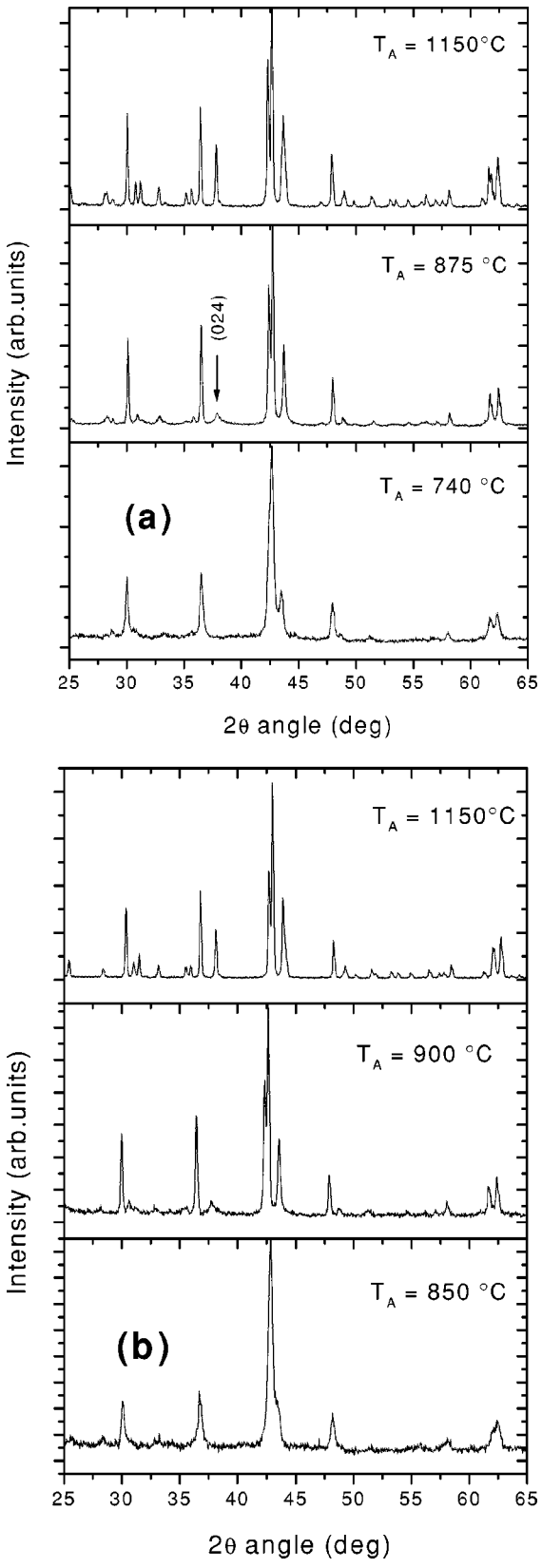

FIG. 1. (a) X-ray diagram for $Sm_2Fe_{16.5}Si_{0.5}$ at $T_A=740$, 875, and 1150 °C. (b) X-ray diagram for $Sm_2Fe_{15}Si_2$ at $T_A=850$, 900, and 1150 °C

the reduced $R\bar{3}m$ cell of Sm_2Fe_{17}, $x=0$, $a'=a_{rho}/\sqrt{3}$ and $c'=c_{rho}/3$ ($a'=4.941$ Å and $c'=4.147$ Å),[11] it is found that c increases and a decreases as you go from Sm_2Fe_{17} to $SmFe_9$. This result is in agreement with the model proposed by Buschow and Van der Goot.[21] It was concluded that the Sm content rules this evolution. The deficient $SmFe_9$ phase which could accept some small stoichiometry deviation from $s=0.33$ up to $s=0.36$–0.38 from the crystallographic point of view, appears as the disordered precursor of the ordered stoichiometric Sm_2Fe_{17} phase.

2. Effect of Si on the P6/mmm $SmFe_9$ *phase*

The structure approach employed here is based on the atom distribution relationship between the atomic positions of the $R\bar{3}m$ structure and those of the hexagonal $P6/mmm$ according to the Si location established previously in the $R\bar{3}m$ Sm_2Fe_{17} phase.[12] The M atom positions of one phase should be as close as possible to those of the other: the $2e$ and $6l$ positions in the hexagonal $SmFe_9$ phase transform, respectively into $6c$ and $18f$. The $3g$ splits for one third into the $9d$ position and two thirds into the $18h$ position in the rhombohedral Sm_2Fe_{17} phase. The $1a$ R position gives rise to the $6c$ R site. It results that the Si location, preferentially in the $18h$ site, is consistent with the exclusive occupation of the $3g$ site. The Rietveld refinements have been performed on the basis of this deduction. In order to clarify the understanding of silicon content in the $P6/mmm$ phase we have converted the x values of nominal $Sm_2Fe_{17-x}Si_x$ to y in $SmFe_{9-y}Si_y$. The values of $x=0.5$, 1, 1.5, 2, and 3 will be respectively replaced by $y=0.26$, 0.52, 0.78, 1.04, and 1.56 in the following. Let us consider first the case of the (A) family obtained after annealing in the range 650–850 °C. The x-ray linewidth deduced from Thompson-Cox-Hastings line profile is typical of nanocrystalline state with autocoherent diffraction grain size varying from 220 to 280 Å for, respectively, $y=1.04$ and 0.52. In Fig. 2 are reported the unit cell parameter variations versus the nominal Si content y. For $y<0.78$, a and c are found to decrease simultaneously with a light slope of -0.32 % per Si atom. For $y\geqslant 0.78$, this decrease becomes four times higher, around -1.2% per Si atom for a while c turns to increase with a slope around $+0.8$ %. For the small Si contents, the Si effect is of the same order of magnitude as that observed in the $R\bar{3}m$ $Sm_2(Fe,Si)_{17}$ structure, a' and c' are poorly affected and decrease as expected upon the substitution of Fe by Si with a smaller size.[12] For $y=0.78$ the behavior is completely different and follows the evolution observed by Buschow and Van der Goot[21] for the Co super stoichiometric $Sm_{1-s}Co_{5+2s}$. We suggest that the Sm content decreases slightly comparatively to $y=0.26$ and 0.52. Some additional Sm atoms are replaced by Fe-Fe dumbbells. The hexagonal phase $P6/mmm$ might not accept any more volume contraction and the light Sm deficiency might balance the decrease that would result from more Si substitution. For $y=1.56$, iron precipitates and additional diffraction lines belonging to $SmFe_2Si_2$ appear on the x-ray diagrams. The cell parameters of the coexisting $P6/mmm$ phase are close to those measured

TABLE I. Atom Wyckoff position and atom occupancy in the $P6/mmm$ structure as a function of the substitution rate s of the rare earth in the $R_{1-s}M_{5+2s}$ alloys.

Atom position		$s=0$ $CaCu_5$	$s=0.22$ $TbCu_7$ (Pearson)	$s=0.33$ 2/17	$s=0.36$ 1/9
1 Sm $(1a)$ 0,0,0	$1-s$	1	0.78	0.66	0.64
2 Fe $(2c)$ $\frac{1}{3},\frac{2}{3},0$	$2(1-3s)$	2	2	0	0
6 Fe $(6l)$ $x,2x,0$	$6s$	0	0	2	2
3 Fe $(3g)$ $\frac{1}{2},0,\frac{1}{2}$	3	3	3	3	3
2 Fe $(2e)$ 0,0,z	$2s$	0	0.44	0.66	0.72

for $y=1.04$ and give evidence of a solubility limit y equal to 1.22. It must be emphasized that the unit cell parameter of the Si substituted $R\bar{3}m$ $Sm_2Fe_{17-x}Si_x$ compounds shows, up to $x=2$, the same trend as for small y contents with a constant Sm stoichiometry.[12] Moreover, the unit cell parameter a of the (A) family alloys, for a given y value, is systematically lower than a', parameter of the reduced $R\bar{3}m$ structure (B) family. On the contrary c is always larger than c'. Figure 3 reports the monotonic decrease $(a'-a)/a'$ and the concomitant monotonic increase $(c'-c)/c'$ versus y, which reflects the Sm deficiency of the hexagonal $P6/mmm$ precursors compared with the homologous rhombohedral alloys. This effect is more pronounced with y increasing and corroborates the Fe enrichment for $y=0.78$ and 1.04 compared to $y=0.26$ and 0.52. The (C) family characterized by the onset of $R\bar{3}m$ extra lines reveals the effect brought about by temperature upon the $P6/mmm$ structure. As an example, consider Fig. 4 for $y=0.52$. After annealing at 750 °C, which corresponds to the temperature leading to the (A) family, a and c are respectively equal to 4.917 and 4.159 Å . After annealing at 875 °C which still induces the (A) family without any $R\bar{3}m$ extra lines, their values reach 4.924 and 4.147 Å . The reduced parameters a' and c' at 1150 ° C (B) region are $a'=4.932$ and $c'=4.145$ Å . This means that a increases towards a' while c decreases towards c'. These evolutions, which follow Buschow's model,[21] corroborate the Sm enrichment of the $P6/mmm$ structure. The 2/17 stoichiometry is approached as the annealing temperature increases. Moreover the (C) family detected in a narrow temperature range can be explained as a mixture of the $P6/mmm$ phase supporting stoichiometry deviations, with unit cell parameters matching the reduced parameters of the $R\bar{3}m$ of Th_2Zn_{17} type structure and the gradual growth of the stoichiometric Th_2Zn_{17} phase.

TABLE II. a and c cell parameters, and R_B, χ^2 factors from the Rietveld fit for $SmFe_{9-y}Si_y$

	$y=0.26$	$y=0.52$	$y=0.78$	$y=1.04$
a (Å)	4.921	4.917	4.904	4.889
c (Å)	4.163	4.159	4.172	4.184
R_B	5.48	6.37	5.80	5.88
χ^2	1.69	1.39	1.87	1.56
s	0.35	0.35	0.36	0.36
$x\{6l\}$	0.291	0.291	0.289	0.291
$z\{2e\}$	0.289	0.290	0.290	0.289

B. Magnetic properties

The Curie temperature T_C of the samples annealed at 750 °C increases from 450 up to 560 K for $y=1.56$ (Fig. 5). This value which is some two degrees higher than that observed for $y=1.04$ within the experimental uncertainty (± 3 K), corroborates the fact that the solubility limit is slightly higher than 1.04 as deduced from the x-ray data. Whatever y, the T_C values are systematically higher by about 30 K than those of the homologous $R\bar{3}m$ compounds.[12] According to Givord and Lemaire[22] R_2Fe_{17} has two kinds of exchange interactions, one positive and the other negative. When the separation within the individual Fe-Fe pairs is smaller than 2.45 Å , the exchange interactions are negative; at large Fe-Fe separations, the interactions are positive. We may interpret the increase of the Curie temperature when silicon atoms replace iron in RFe_9 in terms of a decrease in the negative exchange interactions.[23] However, the increase of T_C might also be explained in terms of electronic effects connected to the filling of the $3d$ band. We will now demonstrate that this is the more likely explanation. The low T_C value in the 2/17 $R\bar{3}m$ structure is commonly attributed to

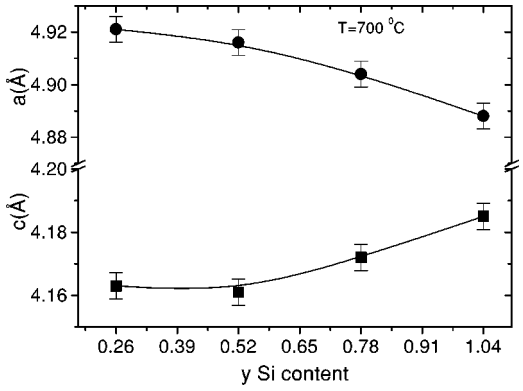

FIG. 2. Unit cell parameters vs silicon content of $SmFe_{9-y}Si_y$

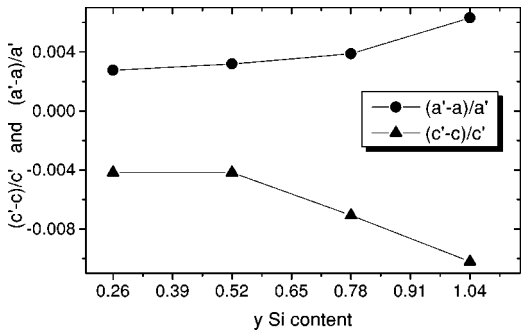

FIG. 3. $(a'-a)/a'$ and $(c'-c)/c'$ vs silicon content of $SmFe_{9-y}Si_y$. The primed and unprimed lattice parameters are, respectively, those of the reduced $R\bar{3}m$ and $P6/mmm$ structures.

the strong negative coupling of the $6c$ Fe atoms within the individual Fe-Fe dumbbells. The separation of these Fe atoms is about 2.36 Å . In the $P6/mmm$ structure $Sm(Fe,Si)_9$, the $(2e)$ Fe atoms are separated by distances slightly larger, at around 2.40–2.42 Å according to the unit cell parameter given in Table II. However, for the same Si content the volume of the reduced $R\bar{3}m$ cell is always higher than the volume of the $P6/mmm$ cell. It results that all inter-atomic distances, except those of the dumbbell pairs and the $3g-6l$ distances derived from the $9d-18f$ distances in the $R\bar{3}m$ structure (and already known to contribute strong negative interactions), are shorter in the $P6/mmm$ structure while T_C is higher. Consequently, the T_C increase of the $P6/mmm$ cell versus y must result from electronic effects. This is consistent with the filling of the iron $3d$ band with the $3p$ electrons introduced by the silicon substitution. Moreover, the effect of this substitution is to push the $3d$ states to higher energy.[24] This effect leads also to an increase in the iron moment as observed from the magnetization data (Fig. 6). The mean magnetic moment per Fe atom, calculated from the saturated moments in the assumption of an opposite free-ion moment on the Sm site, is found to increase from $1.88\mu_B$ for $y=0.26$ to 1.97 for $y=1.04$, some few per cents more than for the $R\bar{3}m$ $Sm_2(Fe,Si)_{17}$ alloys.[12] Such slight improvement of

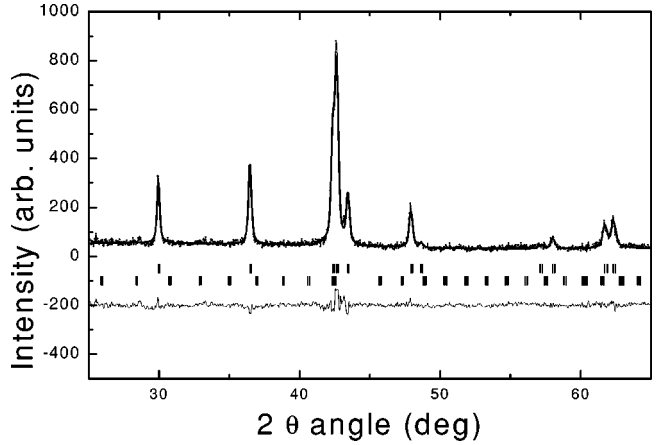

FIG. 4. Rietveld analysis for sample of $SmFe_{9-y}Si_y$, for $y=0.52$. The sets of ticks refer, respectively, to $P6/mmm$ and Sm_2O_3.

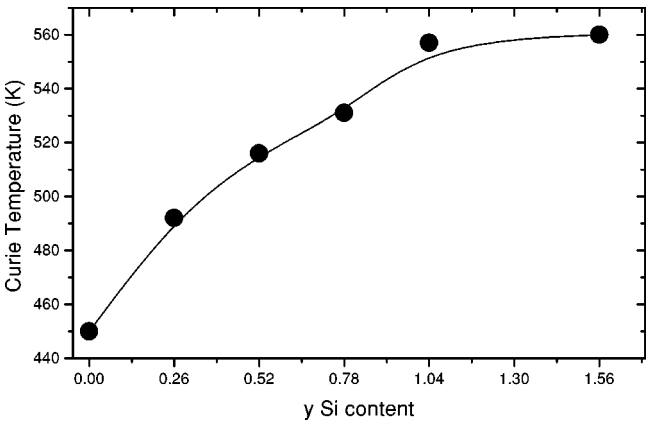

FIG. 5. Curie temperature vs silicon content of $SmFe_{9-y}Si_y$ annealed at 750 °C. The solid line is a guide for the eye.

the magnetic moment per transition metal atom in the $P6/mmm$ structure compared to its homologous $R\bar{3}m$ structure might lead to an enhancement of the anisotropy field in the $P6/mmm$ structure which was previously observed in the Sm_2Co_{17} alloys.[25] The initial magnetization curves [Fig. 6 (inset)] are marked by a low initial permeability with an evident inflection point typical for pinning type materials. This can be related with the doping effect of silicon; thus when the silicon content is increased, the pinning field increases. Responsible for the pinning effects are homogenous precipitates inside the main phase grains, which impede the motion of domain walls where they are located. For precipitates to be effective pins, they must be crystallographically coherent with the matrix and have magnetic properties that differ from those of the matrix phase. They must have the right size and spacing. However, monodomain behavior cannot be excluded, as the diffraction grain size is around 250 Å large for all samples. Nevertheless, the magnetization curves [Fig. 6 (inset)] for $y=0.78$, 1.04 are separated from those for $y=0.26$ and 0.52. One can notice that this behavior corresponds to the change in slope in the unit cell parameter at about $y=0.52$.

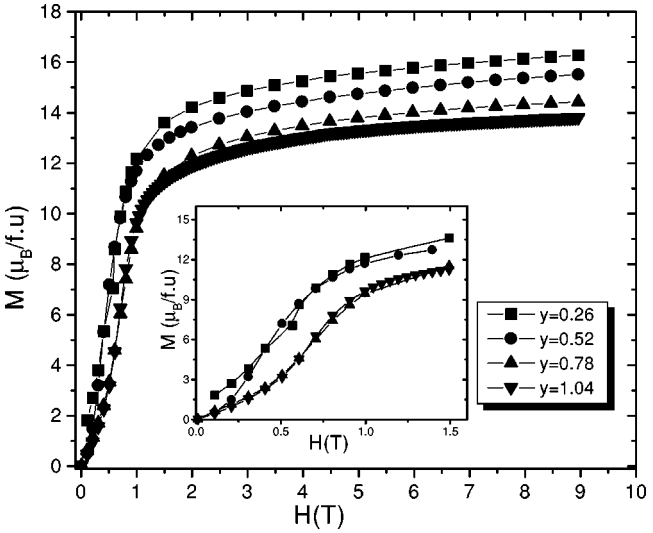

FIG. 6. Magnetization curves of $SmFe_{9-y}Si_y$ powders vs Si content measured at 4.2 K. The initial magnetization curves (inset).

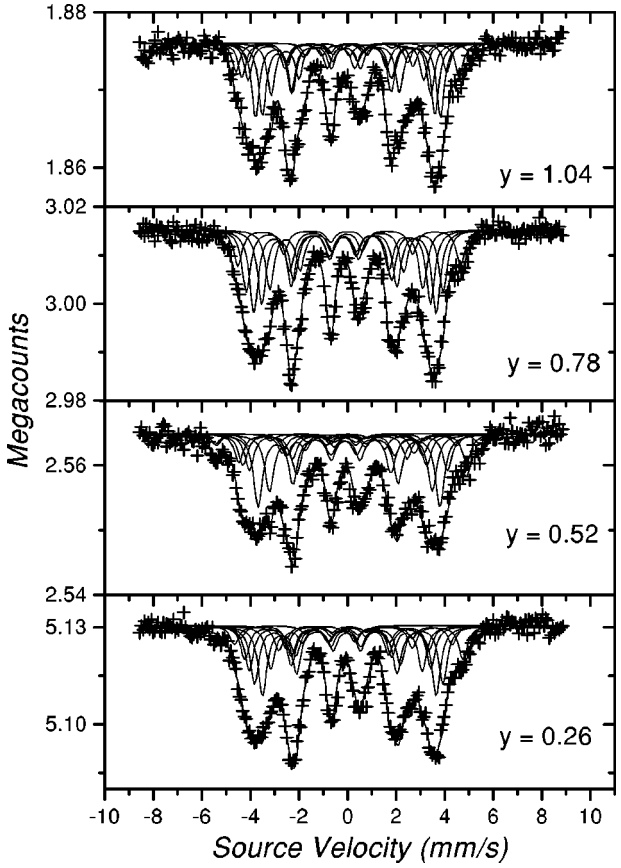

FIG. 7. The 293-K Mössbauer spectra of $SmFe_{9-y}Si_y$.

C. Mössbauer spectra analysis

The Mössbauer spectra relative to the hexagonal phase obtained at room temperature, together with the fits, are shown in (Fig. 7). We must point out that the atomic arrangements are rather complex due on the one hand to the existence of three crystallographic sites and, on the other hand, to the statistical distribution of silicon. Consequently, the experimental spectra result from the convolution of numerous sextets. The interpretation of such spectra is dependent on the choice of physical model justified by pertinent experimental information brought by other techniques like, for instance, x-ray diffraction. Finally all techniques must be self-consistent. The clue of the Mössbauer analysis which we have carried out derives from two criteria.

(i) The possible distinction of the various iron sites, specified by their hyperfine parameters sets δ, H_{HF}, and 2ε, results from a first order perturbation by neighbor atoms (Table III). The smallest number of magnetic sites required for fitting the spectra consistent with a reasonable linewidth around 0.30 mm/s per site; the most pertinent solution.

(ii) The assignment of the hyperfine parameter set of a given sextet to its crystallographic site obeys the relationship between the isomer shift and the Wigner-Seitz cell (WSC) volumes: the larger the WSC volume the larger the isomer shift δ.

In the first step we have calculated, by means of the binomial law, the relative abundances of the Fe families in the various crystallographic sites $2e$, $3g$, and $6l$ with the assumption of silicon in the $3g$ site as given by the Rietveld analysis. The various types of neighboring atoms were considered for a radius equal to 2.76 Å around each atom. They are reported in Table III.

TABLE III. Wigner-Seitz cell volumes and interatomic distances for the hexagonal $P6/mmm$ structure for $SmFe_{9-y}Si_y$ $y=1.04$ as an example, ($a=4.889$ Å , $c=4.184$ Å). The distances are calculated inside a radius of the coordination sphere equal to 2.76 Å .

Site	WSV $(Å)^3$	Distance (Å)	Number of Fe/Si atoms	Notation
$6l$	12.80	2.46	2	6l
		2.45	4	3g
		2.74	2	3g
		2.74	2	2e
$2e$	19.49	2.41	1	2e
		2.60	6	3g
		2.75	6	6l
$3g$	12.87	2.44	4	3g
		2.45	4	6l
		2.60	2	2e

(a) The $2e$ Fe are submitted to the influence of one possible neighbor $2e$ dumbbell according to a statistical distribution of iron and vacancies in the $2e$ site. The closest neighboring site of $3g$ type, more distant, will not be considered.

(b) The $3g$ population can be differentiated by the statistical distribution of Fe and Si on four $3g$ first neighbors. The statistical distribution of two $2e$ Fe in the next neighboring shell, has been neglected.

(c) The $6l$ sites undergo the influence of the set of four $3g$ first neighbors Fe/Si. The effect of one $2e$ dumbbell, in the second neighboring shell, was also neglected.

The WSC volumes have been calculated by means of Dirichlet domains and coordination polyhedra for each crystallographic family. We have used the procedure of radical planes, which results in a space partition without gaps between the polyhedra.[26] Radius values of 1.81, 1.26, and 1.17 Å have been used,[27] respectively for Sm, Fe, and Si.

We have simulated the partial occupation by performing the calculations in a $P6/mmm$ appropriate subgroup in a way that allows the splitting of the partially Si occupied positions. The simplest possibility is given in subgroup $P1$ with $a'=3a$, $b'=3b$ and $c'=2c$, where we had to take into account all atoms corresponding to the fully occupied positions (20 atoms) and one additional atom from one of the other positions. The WSC volumes resulting from such calculation (see Table III) lead to the following volume sequence $V\{2e\}>V\{3g\}>V\{6l\}$, whatever the Si content.

The interpretation of the spectra require two more remarks: the Lamb-Mössbauer factors were set equal for all sites $2e$, $3g$, and $6l$ of the $P6/mmm$ structure, the relative abundance of each sextet line was taken in the ratio 3/2/1 of

TABLE IV. Mössbauer hyperfine parameter for $SmFe_{9-y}Si_y$ for $y=0.52$, as an example, at room temperature. Hyperfine field, H_{HF} (kOe); isomer shift, δ (mm/s); quadrupole interaction, 2ε (mm/s), and relative area, $A(\%)$. Linewidth $\Gamma=0.30$ mm/s

	$2e_0$	$2e_1$	$\langle 2e\rangle$	$3g_0$	$3g_1$	$3g_2$	$\langle 3g\rangle$	$6l_0$	$6l_1$	$6l_2$	$\langle 6l\rangle$
H_{HF}	283	275	281	222	223	192	219	242	204	212	224
δ	0.122	0.035	0.098	0.035	-0.168	0.146	-0.031	0.06	-0.027	-0.0181	-0.027
2ε	0.052	0.015		-0.022	-0.039	-0.030		-0.105	-0.102	-0.108	
A	9.8	3.8	13.6	24.3	18.5	5.4	48.2	19.3	14.7	4.2	38.2

random powders as no texture was observed on the x-ray diagrams. Along the fitting procedure, the relative abundance of the Fe families, calculated with the binomial law were maintained as fixed parameters. Only the abundances higher than 1.8% were taken into account. All other parameters viz. δ, H_{HF}, and 2ϵ were free. In the second step of the refinement, the deduced averaged isomer shift values have been assigned to each site of the $2e$, $3g$, and $6l$ families according to their respective WSC volume sequence. Finally, in the last step of the fit, all hyperfine parameters were free. The solid lines shown in Fig. 7 are the result of the fits with the constraints described above and the resulting hyperfine parameters are given, as an example for $y=0.52$, in Table IV.

Figure 8(a) shows the isomer shift evolution versus y at room temperature for the different sites. For a given y, the sequence observed is $2e>3g>6l$, as assumed from WSC volume correlation. There is an increase for the mean isomer shift of the $2e$ and $6l$ atoms upon silicon substitution, while for the $3g$ atoms it remains quasiconstant. This result can be understood in terms of the preferential silicon atom occupation. The WSC volume reduction which might contribute to an increase in the *s*-electron density at the iron nuclei is widely balanced by the enhancement of the *d*-electron density brought by $3p$ silicon electrons which, in turn, gives rise to a reduction of the *s*-electron density at the iron nuclei. The additional silicon $3p$ electron favors the shielding of the $4s$ electrons. It results in an increase in the isomer shift for the iron nuclei having silicon as first neighbors and no effect for the nuclei that belong to the sites where silicon is located. The $2e$ and $6l$ iron sites have six adjacent $3g$ neighbors while the $3g$ site atoms have only four. The $3g$ atoms with fewest $3g$ neighbors are the least affected by the silicon substitution and their *s* charge density is then not modified. Weak change is observed for the $\delta\{3g\}$. This specific $3g$ site behavior then corroborates the preferential occupation of silicon atoms at this site.

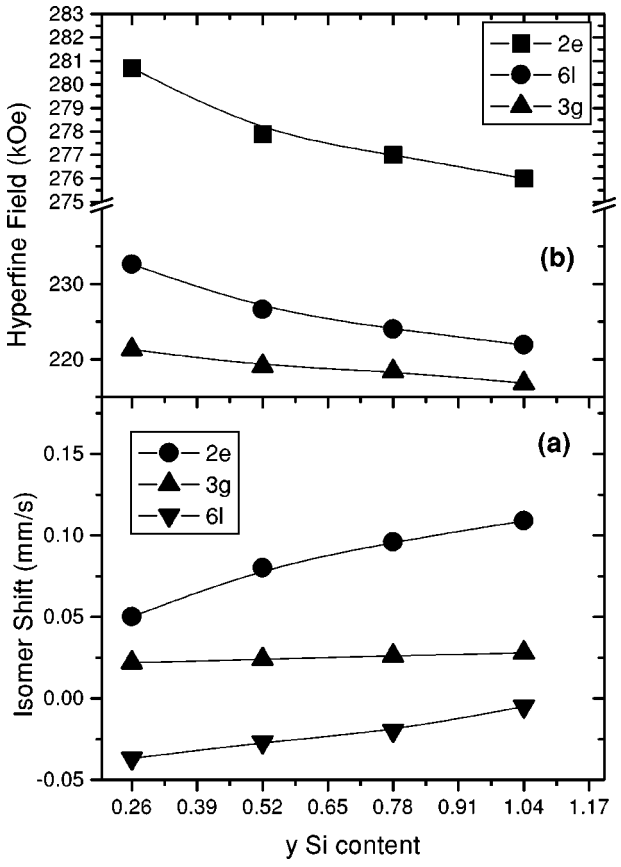

FIG. 8. The compositional dependence of (a) the isomer shifts and (b) the hyperfine fields for $SmFe_{9-y}Si_y$. The plotted data are the weighted average values for each three sites.

The mean hyperfine fields [Fig. 8(b)] decrease with Si content as observed in the $R\bar{3}m$ $Sm_2(Fe,Si)_{17}$ compounds. The same explanation can be given. It results from the competition between negative core polarization term and the positive term arising from $4s$ conduction electrons. The following hyperfine field classification $H_{HF}\{2e\}>H_{HF}\{6l\}>H_{HF}\{3g\}$ is obtained. As a conclusion of the Mössbauer analysis, the consistency of the results corroborates the crystallographic deductions.

IV. CONCLUSIONS

We have studied the structure and intrinsic magnetic properties of $Sm(Fe,Si)_9$, the $P6/mmm$ precursor of the $Sm_2(Fe,Si)_{17}$ $R\bar{3}m$ phase. The approach to the $P6/mmm$ precursor structure results from modifications of the stoichiometric RM_5 phase of $CaCu_5$ type towards *R* substoichiometric RM_9 compounds.

The x-ray diagrams were interpreted according to the relationship between the atom positions in the stoichiometric 2/17 $R\bar{3}m$ phase and those of the hexagonal $P6/mmm$ structure. The Rietveld refinements have been performed with Si located in $3g$ sites.

At a given annealing temperature, the Si enrichment in-

duces a change of slope in the unit cell parameter evolution, confirmed by initial magnetization curves. For small Si content ($y \leqslant 0.52$), the unit cell parameters decrease smoothly upon the Si substitution. From $y=0.52$ up to y slightly higher than 1.04, which corresponds to the solubility limit of Si in the $P6/mmm$ structure, the unit cell parameter behavior gives evidence of a small iron enrichment around 1/9 corroborated by the Rietveld structure refinement. At a given Si content the evolution of unit cell parameters versus annealing temperature from hexagonal towards rhombohedral structure is attributed to Sm enrichment.

The Curie temperatures are systematically 30 K higher than those of the homologous $R\bar{3}m$. They increase with Si content. They are mainly relevant to electronic effects more pronounced than in the $R\bar{3}m$ structure 2/17, and connected to a measured Fe moment enhancement of some percent with regards to the $R\bar{3}m$ structure. Moreover, the initial magnetization curves can be explained either by pinning model or monodomain behavior.

The WSC volumes were calculated with a specific code using the group $P1$. The statistical occupation of the Fe dumbbell and the partial Fe/Si substitution of the $3g$ sites were described by the binomial law.

The Mössbauer hyperfine parameter assignment was performed on the basis of their correlation with the WSC volumes. The isomer shift of the $3g$ sites remains quasi-constant with Si content in agreement with the x-ray analysis and corroborates the preferential Si $3g$ occupation. The mean hyperfine field and the hyperfine field of each crystallographic site decrease with the Si content, as shown previously in the $R\bar{3}m$ $Sm_2(Fe,Si)_{17}$ alloys.

ACKNOWLEDGMENTS

The authors wish to thank Professor V. Pop for his kind assistance for the magnetization measurement, and Dr. V. Lalanne for her technical help in the sample preparation.

[1] H. Fujii, K. Yamamoto, K. Tatami, and M. Akayama, *in Proc. second Int. Symp. on Physics of Magnetic Materials* (International Academic, Beijing, 1992).
[2] A. Handstein, M. Kubis, L. Cao, B. Gebel, and K. H. Muller, J. Magn. Magn. Mater. **192**, 281 (1999).
[3] L. Wei, W. Qun, X. K. Sun, Z. Xing-guo, Z. Tong, Z. Zhi-dong, and Y. C. Chuang, J. Magn. Magn. Mater. **131**, 413 (1994).
[4] H. T. Kim, Q. F. Xiao, Z. D. Zhang, D. Y. Geng, Y. B. Kim, T. K. Kim, and H. M. Kwon, J. Magn. Magn. Mater. **173**, 295 (1997).
[5] J. Shield and B. E. Meacham, J. Appl. Phys. **87**, 2055 (2000).
[6] B. E. Meacham, J. Shield, and D. J. Branagan, J. Appl. Phys. **87**, 6707 (2000).
[7] W. Coene, F. Hakkens, T. H. Jacobs, D. B. de Mooij, and K. H. J. Buschow, J. Less-Common Met. **157**, 255 (1990).
[8] S. Zhang, H. Zhang, B. Shen, T. Zhao, F. de Boer, and K. H. J. Buschow, J. Appl. Phys. **87**, 1410 (2000).
[9] M. Katter, J. Wecker, and L. Schultz, J. Appl. Phys. **70**, 3188 (1991).
[10] A. Teresiak, M. Kubis, N. Matteru, M. Wolf, and K. Müller, J. Alloys Compd. **274**, 284 (1998).
[11] C. Djéga-Mariadassou and L. Bessais, J. Magn. Magn. Mater. **210**, 81 (2000).
[12] C. Djéga-Mariadassou, L. Bessais, A. Nandra, J. M. Grenèche, and E. Burzo, Phys. Rev. B **65**, 014419 (2001).
[13] H. M. Rietveld, Acta Crystallogr. **22**, 151 (1967).
[14] H. M. Rietveld, J. Appl. Crystallogr. **2**, 65 (1969).
[15] J. Rodríguez-Carvajal, M. T. Fernandez-Diaz, and J. L. Martinez, J. Phys.: Condens. Matter **3**, 3215 (1991).
[16] J. Rodríguez-Carvajal, Physica B **192**, 55 (1993).
[17] L. Bessais and C. Djéga-Mariadassou, Phys. Rev. B **63**, 054412 (2001).
[18] L. Bessais, S. Sab, C. Djéga-Mariadassou, and J. M. Grenèche, Phys. Rev. B **66**, 054430 (2002).
[19] D. Givord, J. Laforest, J. Schweizer, and F. Tasset, J. Appl. Phys. **50**, 2008 (1979).
[20] P. Villards and L. D. Calvert, *Pearson's Handbook of Crystallographic Data for Intermetallic Phases* (A S M International, 1991).
[21] K. H. J. Buschow and A. S. V. der Goot, J. Less-Common Met. **14**, 323 (1968).
[22] D. Givord and R. Lemaire, IEEE Trans. Magn. **MAG-10**, 109 (1974).
[23] Z. W. Li, X. Z. Zhou, and A. H. Morrish, Phys. Rev. B **51**, 2891 (1995).
[24] M. Z. Huang, W. Y. Ching, and Z. Q. Gu, J. Appl. Phys. **81**, 5112 (1997).
[25] H. Saito, M. Takahashi, T. Wakiyama, G. Kido, and H. Nakagawa, J. Magn. Magn. Mater. **82**, 322 (1989).
[26] E. Koch and W. Fischer, Z. Kristallogr. **211**, 251 (1996).
[27] E. Teatum, K. Gschneider, and J. Waler, US Department of Commerce Washington DC **LA**, 2345 (1960).